*J. Fluid Mech.* (1982), *vol.* 119, *pp.* 323–345
*Printed in Great Britain*



# Computer analysis of a high-speed film of the plane turbulent mixing layer

By MIGUEL A. HERNAN†
School of Aeronautics, Universidad Politecnica de Madrid, Spain
AND JAVIER JIMENEZ‡
UAM–IBM Scientific Center, P. Castellana 4, Madrid, Spain

(Received 15 April 1981 and in revised form 18 November 1981)

To evaluate the usefulness of digital image analysis in extracting quantitative information from flow pictures we have studied a 16 mm ciné film of a turbulent mixing layer. A sequence of 373 frames is digitized and analysed to isolate and measure the concentration eddies that constitute the large structure and to follow their individual evolution in time. As a result, statistics are given on the life history of the eddies, the structure of the amalgamation process and the amount of entrainment, as measured by area change, due to amalgamation as compared to the total. It is found that most of the entrainment occurs during the normal life of eddies and not during pairing. Mixing intermittency is computed from the observed shape of the eddies and seen to compare well with previous measurements. The significance of these results in modelling the mixing layer is discussed briefly and some comments are given on the general usefulness of the techniques presented.

## 1. Introduction

Visual information has always been important in fluid mechanics. Nowhere has this been clearer than in the study of the large-scale structures in turbulent shear flows. Although it had been known for some time that large eddies were important in those flows and that their behaviour was not strictly disordered (Townsend 1956), the full realization of their quasi-deterministic nature and of their importance in ordering the flow had to wait for the beautiful shadowgraphs contained in Brown & Roshko (1974). Unfortunately it has been difficult up to now to extract more than qualitative information from flow-visualization pictures. The reasons are several: firstly the photographic processing of pictures is slow and cumbersome, secondly it is difficult in many cases to obtain accurate measurements of optical density and dimensional data from pictures, and finally the amount of information, relevant or irrelevant, contained in a single image, and even more so in a ciné film, is so great as to tax the processing ability of a human observer.

Automatic digital image processing has been developed in the last two decades to cope with similar problems in areas like remote sensing and medical technology, and

† Present address: Department of Aeronautics, California Institute of Technology, Pasadena, U.S.A.
‡ Present address: Department of Applied Mathematics, California Institute of Technology, Pasadena, U.S.A.

by now there exists a large repertory of techniques to process different types of images. These techniques can be broadly classified in two categories. Interactive analysis depends directly on a human operator who trains the computer continuously and is responsible for judging the meaning of the resulting processed image; in this type of analysis the computer acts like a sophisticated photographic laboratory whose main object is to modify and display the images in a form more convenient to the human observer. In fully automatic processing, usually known as image analysis, the aim is to write programs that substitute for the observer in part of the course of understanding the image; examples are the automatic extraction of important features and the segmentation of pictures. The result of most of these activities is not so much a new, processed, image but data given in final form as plots or print-outs of the desired properties. Both types of analysis are complementary, and they usually correspond to different phases of the processing of a given picture.

We have explored the application of these processing techniques to the analysis of flow-visualization pictures. The example chosen is a high-speed ciné film of the plane mixing layer. Here the interesting data refer to the Lagrangian evolution of the large structures that dominate the concentration field. This information is clearly contained in the film but has been difficult to extract by conventional means, owing mainly to the sheer amount of work needed to process the many frames that constitute the data. This made the problem a good example in which computer processing might be of interest.

The techniques used in analysing the film are presented in some detail in §§2–4. The results are presented in §§5–7. First the Eulerian statistics of eddy shape and position are obtained, and we then address the problem of which is the evolution of a single eddy along its lifetime. Finally, the significance of the results from the point of view of mixing-layer modelling are discussed briefly, and some considerations are given on the advantages and limitations of the processing method in this and other situations in fluid mechanics.

## 2. Digitization and preprocessing

The film containing the original data is digitized using a Perkin Elmer 1010 MP flat-bed microdensitometer, whose operation is explained below. This instrument produces computer compatible tapes containing the digital representation of individual photographic negatives. These tapes are read and analysed by an IBM 370/158 mainframe computer. As noted above the analysis produces either completely automatic results, given in the form of plots or tables, or interactive programs; the interaction is done by means of a standard CRT computer terminal plus a RAMTEK 9551 graphic station in which it is possible to display digital images or line drawings on a colour screen and to select points on the screen using a moving cursor; this terminal is connected on-line to the host computer and it is therefore possible to select interactively the type of analysis to be done or the items to be displayed.

The data used in the analysis are contained in a 16 mm shadowgraph ciné film taken by L. P. Bernal at the Graduate Aeronautical Laboratories of the California Institute of Technology. The experimental apparatus has been described in Brown & Roshko (1974). The mixing layer is established between a high-speed stream of nitrogen ($U_1 = 10$ m/s) and a low-speed one ($U_2 = 3{\cdot}8$ m/s) of a He–Ar mixture adjusted so

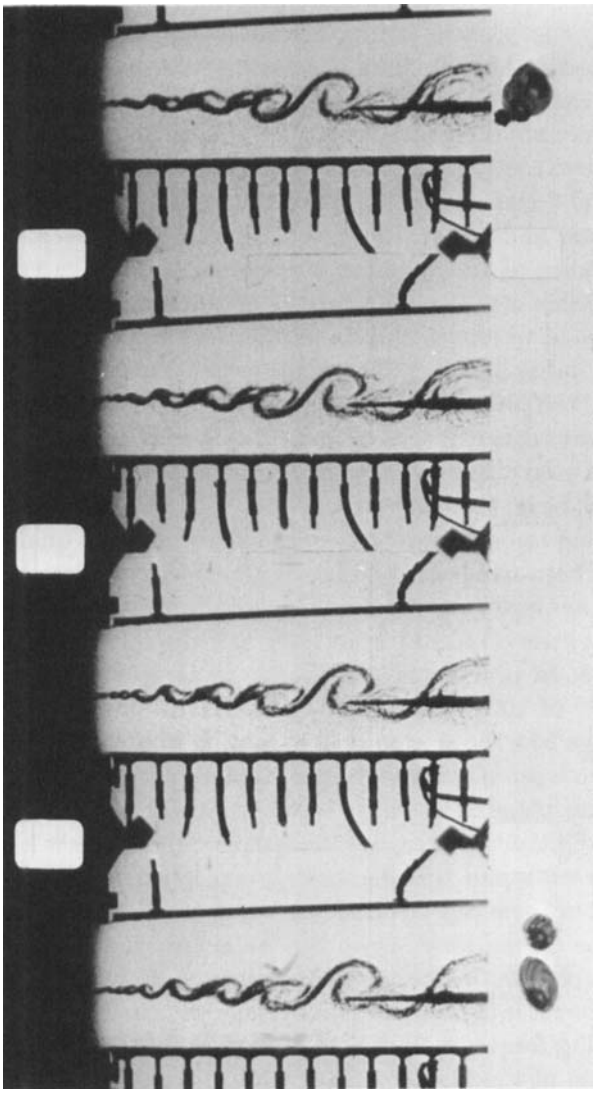

FIGURE 1. A few frames from the original ciné film used in this paper.

that its density is equal to that of nitrogen. The length of test chamber shown in each frame (figure 1) is about 160 mm, so that the Reynolds number based on this length and on the velocity difference is about 800000. Konrad (1976), studying sets of simultaneous plan and side shadowgraphs of a mixing layer with similar parameters in the same experimental apparatus, discovered the existence of a transition near $x = 20$ mm which he associated with the appearance of three-dimensionality in the flow; therefore most of the length of the layer shown in this film probably contains appreciable amounts of three-dimensional structure.

The shadows that appear in the film are proportional to the integral along the span of the second derivative (Laplacian) of the index of refraction in a plane perpendicular to the light beam, and therefore mark the interface either between fresh fluid of both free streams or between one stream and the well-mixed fluid inside the eddies. The

spatial resolution of the data can be estimated from the thickness of the shadow produced by the very sharp discontinuity present at the exit of the splitter plate, which in our case is about 100 $\mu$m on the film plane, setting a limit of 1·5 mm on the flow plane to the smallest possible detail that can be extracted from the film.

Individual frames are digitized using the microdensitometer. In this instrument a light beam of known section and intensity is focused on a photographic negative and the amount of light transmitted through the negative is measured with a photomultiplier, digitized and written on tape; this value is proportional to the average optical transmittance of the negative over the area illuminated by the beam. The shape and size of this area can be adjusted by clipping the section of the incoming beam with a series of windows, and its position can be scanned over the film by displacing the glass table carrying the negative. By sampling this scanned signal at discrete intervals, the photographic image is transformed into a numerical matrix in which each element represents the transmittance of a finite picture element (pixel), and which can be used either to reconstruct the image on the graphic terminal or to analyse its properties on the computer.

The relation between the scanning parameters and the quality of the resulting digital image has been treated in the literature with some detail (Pratt 1978, p. 93). The basic result, analogous to the Nyquist criterium for one-dimensional signals, is that the sampling interval has to be at least half the shortest wavelength present in the original image. In practice it is advisable to sample a little more densely, and, given our estimate of 100 $\mu$m as the finest detail in the negative, we have sampled every 25 $\mu$m using a 25 $\times$ 25 $\mu$m square illuminating window. Therefore every negative is decomposed into a set of non-overlapping square elements, each 25 $\mu$m on the side (0·4 mm on the flow plane).

In the original digitization a part of the test chamber walls is always included. The sharp edge of the walls can then be used to register geometrically all the digitized frames, so that all of them can be considered to share a common frame of reference to within a difference of one pixel. Once the walls are used for this purpose they are clipped out of the picture to save processing time.

Also of some interest is the temporal sampling rate. At the centre portion of the test chamber the passing frequency of the eddies was estimated to be around 300 Hz, or, as the framing rate of the film was 2000 frames/s, one eddy every six frames. The shortest lifetime of an individual eddy was expected to be about half this value (Brown & Roshko 1974), and it was therefore decided that analysing only one frame every three would not miss a significant portion of the life histories. Since in this period an eddy moves only about half its own length, the resolution is still good enough to track the motion of the eddies between frames. In this way we digitized a series of 373 frames, corresponding to 1119 consecutive frames of the original movie and to a total test time of about 0·5 s. This sequence was chosen towards the end of the run so that the camera speed would be as close as possible to its nominal value. Still this speed is only known to within 15 %, and is the limiting factor in the accuracy of the results presented here.

A false-colour representation (Pratt 1978, p. 333) of one frame is shown in figure 2 (*a*) (plate 1). Several problems are immediately apparent. The illumination is not very uniform, producing an optical transmittance gradient on the background, vertical scratches appear across the pictures, and, very prominently, an aspirating probe is

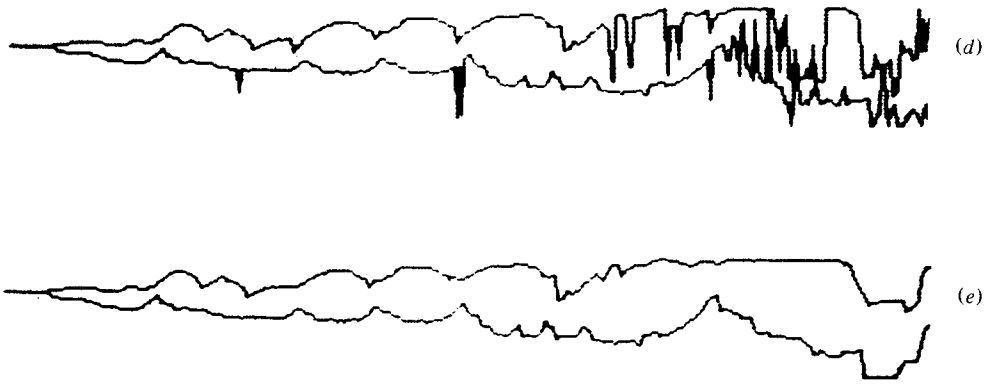


FIGURE 2. Stages in preprocessing one frame (for (*a–c*) see plate 1): (*a*) digitized image; (*b*) filtering; (*c*) thresholding; (*d*) edge detection; (*e*) edge smoothing.

included in the flow, making the interpretation of the downstream part of the layer difficult in some cases.

Fortunately the vignetting and the scratches are essentially vertical zones of uniform illumination which can be estimated by averaging a few lines of the image corresponding to the free streams and later subtracted from the rest of the picture. The result is shown in figure 2(*b*) (plate 1). In this figure the probe has also been removed; because the probe body is a completely opaque object, its optical transmittance is usually somewhat lower than the darkest parts of the mixing region, and is easily located and substituted by values corresponding to the free stream in that part of the image. The resulting rectangular 'ghost' can be seen in figure 2, but its intensity is far from the values associated with the mixing region and does not interfere with the analysis.

## 3. Data compression and segmentation

The image resulting from the operations in §2 is already comparatively noise-free and shows a clear difference between the mixing region and the background, but it contains too much unnecessary information. Since we are only interested in the shape of the mixing region we do not need such details as the transmittance distribution within or outside the layer, and a simpler and equally useful image can be obtained by defining a threshold such that all pixels with low transmittance are classified as mixing fluid while the rest are defined as free stream (figure 2*c*, plate 1). Because the concentration interface thickens downstream owing to either turbulent diffusion or to the spanwise integration of the three-dimensional structure, the contrast of the film changes within each frame and a slightly variable threshold has to be used in the classification; this is easily done by dividing the image into vertical zones, using a clustering algorithm to find an optimum classification for each zone, and interpolating a smoothly varying threshold for the whole image (Chow & Kaneko 1972).

The classified picture can be simplified further by retaining only the outline defined by the upper and lower transitions between the two types of fluid. The easiest way is to scan each column vertically, and to note the first and last appearance of a pixel containing mixing fluid; however, in practice the edges obtained in this way show

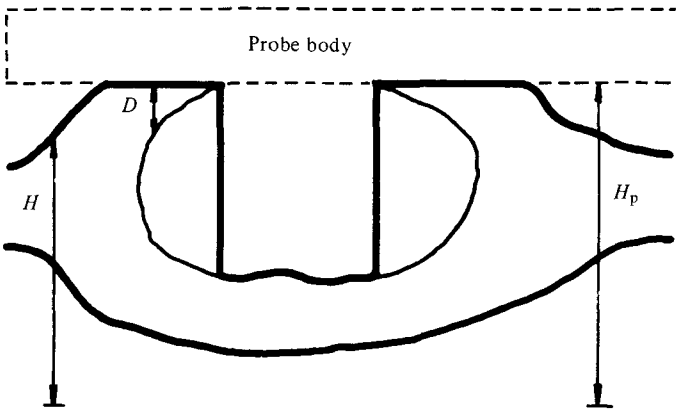


FIGURE 3. Gap left in the outline of the mixing region by the intersection of the probe body.

many peaks and irregularities due to stray misclassified pixels in the free streams and to gaps in the outline (figure 2*d*), and some further processing is necessary. A particularly common and grave problem arises in those frames in which the probe body intersects the mixing region, producing a gap in the upper edge of the region which is reflected as a large 'hole' in the outline. While such a gap cannot really be remedied, it can be recognized and interpolated, and, since the intersection of the probe is usually shallow, the resulting outline is still a useful approximation to the original layer.

The way this recognition is done is a good example of the syntactic methods of pattern analysis. When the edges are extracted, not only their position but their thickness is noted. The expected shape of a probe intersection is shown in figure 3; what we are looking for is a segment in which the position of the upper edge coincides with the lower limit of the probe, which is known from previous processing, and where a sudden dip is preceded and followed by points in which the thickness tapers to zero. Similar definitory rules can be given for such other defects as spikes due to 'salt-and-pepper' noise in the background, dust spots in the negative and small pores in the mixing region. In all these cases the feature being sought begins and ends with a sudden jump in the position of one of the edges, and, if we use those jumps as the end points of segments in which to break the outline, we can use the segments as building blocks of a description of the features that can be easily detected by the computer. It is useful to consider these blocks as 'phonemes' in a formal language, and the descriptive rules as the 'grammar' describing which phonemes can be concatenated to form complex words, and which is the meaning of those words. Later an automaton can be designed to 'understand' the grammar, recognize the words and act accordingly (Fu 1974; Pavlidis 1977). Thus the probe gap can be described by the sequence (see figure 3)

$$\langle H = H_p;\ D \to 0\rangle \langle \text{jump down}\rangle \ldots \langle \text{jump up}\rangle \langle H = H_p;\ D = 0\rangle,$$

recognized and interpolated; the same type of analysis can be used to treat dust spots, etc. The result can be seen in figure 2 (*e*) in which the outline has already been smoothed and is ready for further processing.

It is important to realize the amount of information compression achieved up to now. The original images are matrices containing $120 \times 417$, or 50000, elements each,

while the two edges that are the end result of the processing can be coded into just $2 \times 417$ co-ordinates. In this process much information has been thrown away; by discarding it we risk neglecting something that might have been useful in classifying the coherent eddies, but we get a much smaller data set that can be treated by more complex algorithms.

The next step is to describe the shape of the interface, as contained in the two edges, in term of elements (eddies) which are of immediate interest in fluid mechanics. This is done in three stages. First the mixing layer is segmented, by means of syntactic analysis, in term of 'bulges', local fattenings that are likely candidates for coherent structures, next these segments are classified as eddies or braids according to their shape, and finally an attempt is made to improve this classification by merging neighbouring segments and checking the properties of the resulting unions. A detailed description of these algorithms will be given in a separate paper.

At the end of this process we get what we consider to be the final population of eddies. As part of the process each eddy is fitted to an ellipse which approximates it in the least-square sense and which can be used to represent its shape and position. These ellipses will form the raw material for all the statistics of Eulerian eddy behaviour as well as the input for the temporal-correlation step that organizes the eddies into coherent histories and builds the $(x,t)$-diagram. In fact, from now on these ellipses will be the only information retained from the mixing layer. The result of processing two frames is shown in figure 4 (plate 1).

## 4. Time correlation

Tracking the eddies from frame to frame is now relatively simple. The convection velocity is known to be approximately equal to the average of both free-stream velocities, and the size and shape of the representative ellipses is not expected to change too much in the interval between frames. It is therefore only a matter of extrapolating the ellipses from one frame to their expected positions in the next one and of looking for something of roughly the right size in roughly the right position.

Since eddies move mostly in the streamwise direction we can represent, for the purpose of this section, a frame by a horizontal line in which eddies are marked by segments that are the projections of the ellipses on that direction. When these segments are translated downstream by the amount corresponding to one frame interval they should overlap approximately with the representation of the next frame (see figure 5). When that happens we can assign ascendency–descendency relationships among eddies and organize them into coherent histories spanning several frames.

Amalgamations and processing errors complicate the problem slightly. We assume that the overlap between two segments is measured by the quantity

$$w = \text{length of segment intersection/length of union};$$

then any time that two segments in subsequent frames (once translated appropriately) show an overlap different from zero we can, in principle, postulate a descendency relationship between the eddies. This is especially clear in those cases in which an eddy can be assigned only a single 'child' or a single 'parent'; there are, however, occasions in which we get what appear to be multiple children or parents for a segment. Eddies with multiple parents are easily interpreted as the result of amalgamations, and

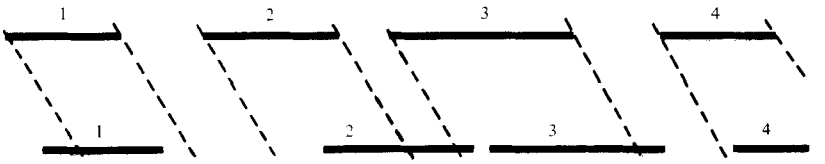


FIGURE 5. Correlation of eddies between consecutive frames. Numbers are identifiers for individual histories.

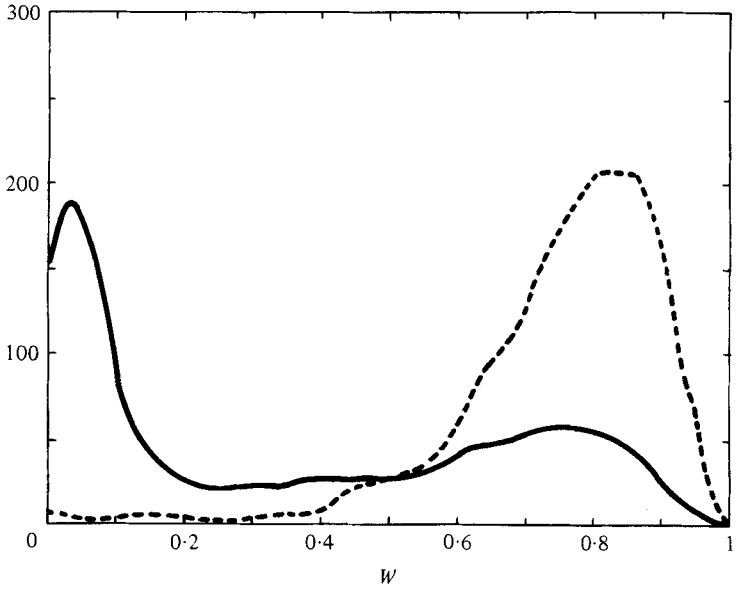


FIGURE 6. Histograms of segment overlap for eddy pairs involving a single possible ascendent (dashed) or several ascendents (solid).

those with multiple children as the result of splittings; care should be exercised, however, to distinguish these phenomena from accidental contacts between eddies that have no real historical relation between them.

Figure 6 shows histograms of the overlaps observed. The dashed line refers to segments having only one parent in the preceding frame; in this case most pairs show a large overlap ($w = 0{\cdot}5$), and the assignation can be done with confidence. The solid line represents those cases in which one eddy contacts at least two parents. There is now a larger range of overlaps, but the most striking feature is the large peak of the histogram in the region of glancing contacts ($w < 0{\cdot}2$). It is easy to interpret this peak as accidental contacts between eddies and their neighbours, and indeed the visual observation of a few cases confirms this interpretation.

We can therefore conclude that segments with an overlap greater than 0·2 are likely to be related historically, while those without overlap or with one smaller than 0·2 are unrelated. In this way eddies can be organized into coherent histories, each history being a sequence of eddies related historically to one another and beginning and ending either when no ascendent or descendent is available or in an amalgamation or splitting. Furthermore, a descendency relation is also established among histories by the amalgamations and splittings, and the whole $(x, t)$-diagram can be drawn.

Some extra processing is necessary to remedy the effects of the classification errors

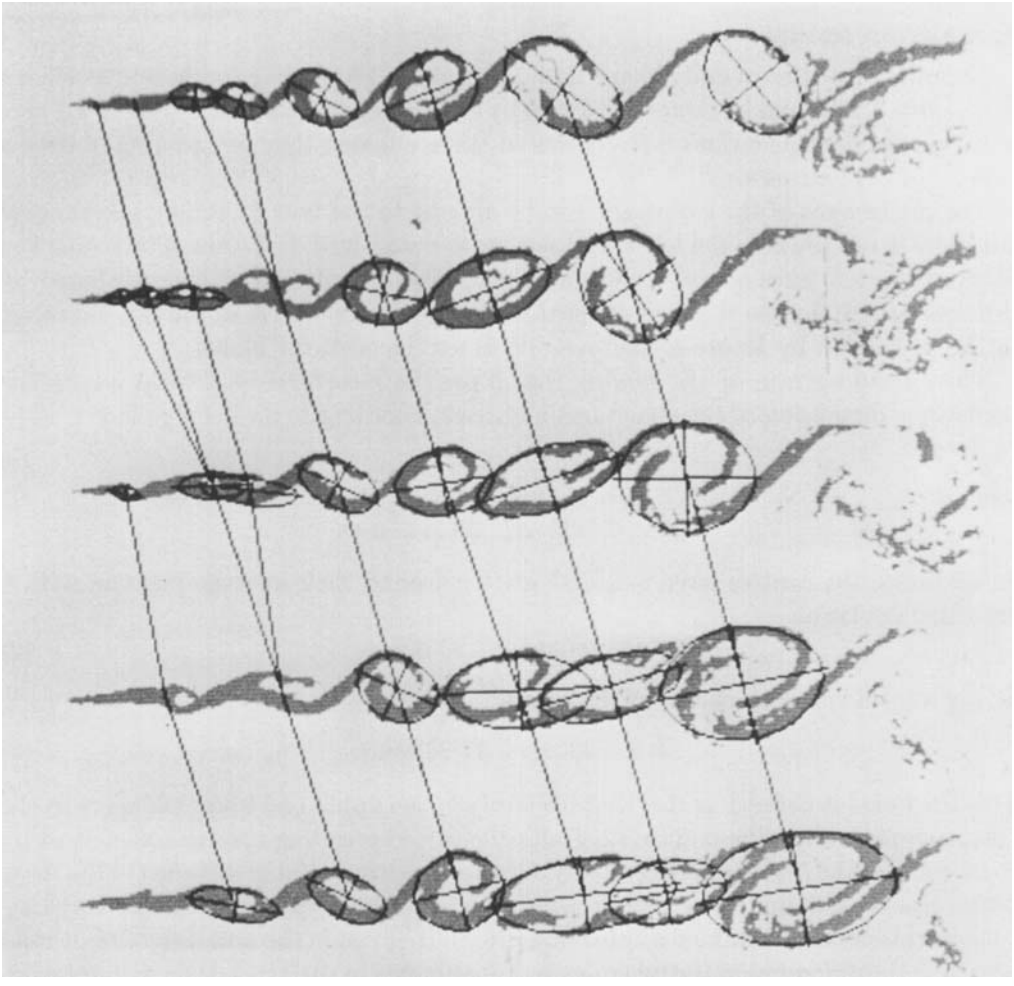

FIGURE 7. A part of the final $(x, t)$-diagram showing several amalgamations; note the tripling on the left of the picture.

committed during the segmentation step. There, some segments of the layer are left unclassified on account of the difficulty in recognizing their shapes. These segments leave gaps in the sequence of eddies representing one frame, and it happens occasionally that a history can be continued by assuming the existence of an eddy of the appropriate size in such a gap. These occasions are especially easy to recognize when there are eddies at the proper positions in the frames just before and after the one to be interpolated, and when moreover the size and position of the gap are such as to permit the interpolation. The algorithm used in our analysis inspects sequences of four consecutive frames, allowing the interpolation of up to two consecutive gaps. A part of the $(x, t)$-diagram drawn in this way is shown in figure 7.

## 5. Eulerian results

Eulerian statistics of eddy shape and position are the easiest to obtain. As shown before, the eddies can be represented well by ellipses, and the statistics presented here will refer to the dimensions and centres of these ellipses; they are computed over a sample of 2214 structures.

The major axes of the eddies tend to be aligned to the flow direction; the average tilt is 0·078 rad towards the low-speed side, with a standard deviation of 0·29 rad. The ratio of the two axes is $1{\cdot}92 \pm 0{\cdot}67$, which agrees well with the values predicted by Jimenez (1980) for the shape of concentration structures, and is in the general range of the ones given by Moore & Saffman (1975) for the vorticity blobs.

The spreading rate of the mixing region can be measured in several ways. The transverse dimension of the structures increases according to an average law

$$\delta_s = 0{\cdot}305\alpha(x + 11{\cdot}3 \text{ mm}), \tag{1}$$

where

$$\alpha = (U_1 - U_2)/(U_1 + U_2) = 0{\cdot}45.$$

In addition, the centres have a lateral scatter around their average position with a standard deviation

$$\sigma = 0{\cdot}038\alpha(x + 30 \text{ mm}), \tag{2}$$

giving a total visual thickness of the region

$$\delta = 0{\cdot}335\alpha(x + 17{\cdot}32 \text{ mm}). \tag{3}$$

This thickness is defined as the distance between the upper and lower tangents to the ellipses representing the eddies. Basically the same spreading rate was measured by Brown & Roshko (1974) as $0{\cdot}38\alpha$ and by Jimenez, Martinez-Val & Rebollo (1979*a*, *b*) as $0{\cdot}39\alpha$. Koochesfahani *et al.* (1979) measured the scatter of the centres of the vorticity concentrations, and obtained a spreading rate that, given in the notation of (2), would be 0·004; the difference in the two rates is probably due to their eddy-selection method, which specifically excludes eddies in the process of pairing. The various spreading laws given above have different virtual origins, although not widely so; somewhat arbitrarily we have chosen the one in (1),

$$x_v = -11{\cdot}3 \text{ mm}, \tag{4}$$

to normalize all the results concerning eddy evolution, and this will be the value used below.

The distance between adjacent eddy centres, when made non-dimensional with the arithmetic mean of the downstream co-ordinates of the two eddies, has a smooth histogram (figure 8) with a mean value

$$\frac{\lambda}{\alpha(x - x_v)} = 0{\cdot}578 \pm 0{\cdot}193, \tag{5}$$

which is in good agreement with previous measurements (Winant & Browand 1974; Brown & Roshko 1974). When the same quantity is represented without any normalization the histogram presents discrete peaks corresponding to the most common values of eddy wavelengths (figure 9). Taking as base value the peak marked as I in

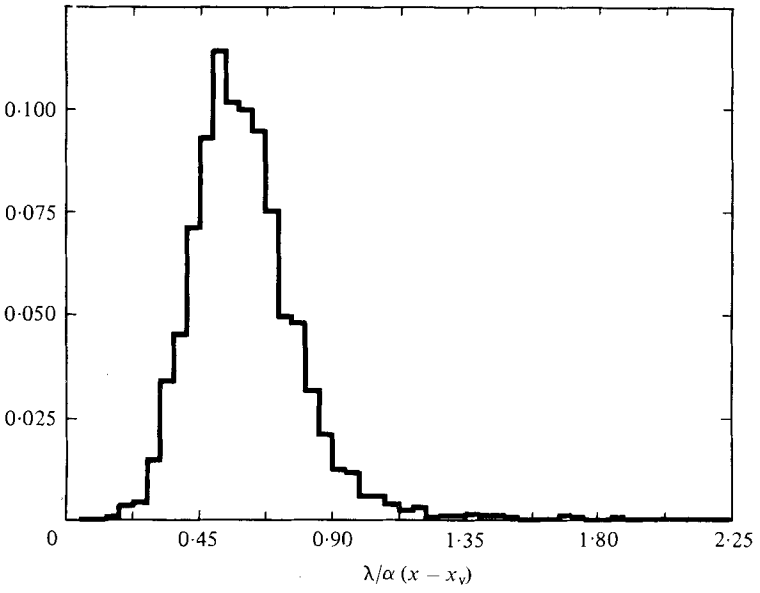


FIGURE 8. Frequency distribution for normalized eddy wavelengths; sample size = 2405.

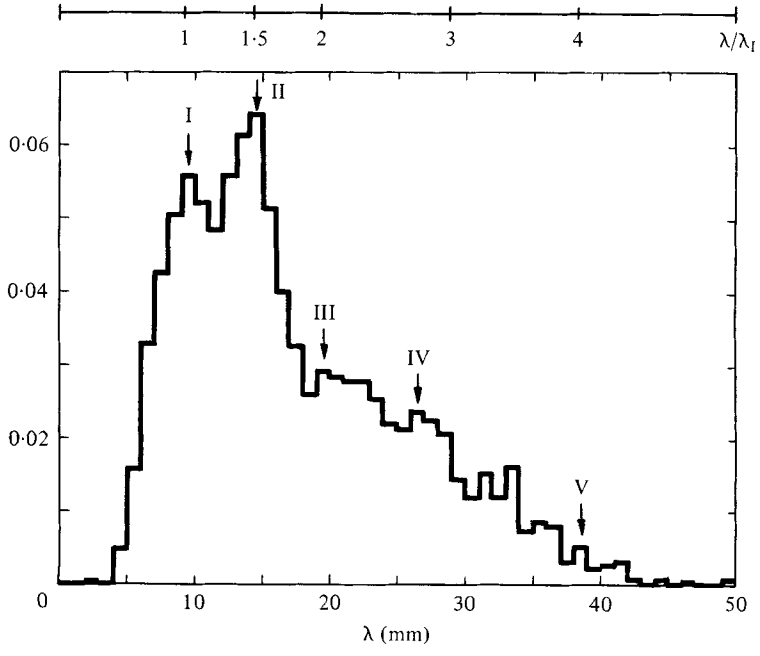


FIGURE 9. Frequency distribution for eddy wavelengths without normalization. Note peaks in the distribution.

the figure, those marked as III and V have wavelengths twice and four times bigger, which can be easily explained as the result of doubling through amalgamation. The intermediate peaks (II and IV) correspond roughly to factors of 1·5 and 3, and they probably arise from the amalgamation of eddies belonging to different generations; thus an eddy of size one, when paired with a previously doubled eddy of size two, will

give something of size roughly equal to three. This mechanism will, in time, give rise to eddies of many intermediate sizes besides the basic sequence 1, 2, 4, ..., and will contribute to the randomization of the layer. In fact, the evolution of the relative simplicity of figure 9 at short wavelengths to the more complex structure at longer ones (downstream) can be traced through the effect of these fractional interactions. Similar results were obtained by Jimenez *et al.* (1979*a*) using anemometry data.

## 6. Amalgamations

Except for interactions and amalgamations it is possible to consider the eddies as individual structures, with temporal as well as spatial coherence, whose characteristics evolve during their lifetimes. Before this evolution can be studied it is important to investigate the events marking the limits of this coherence. Two different mechanisms have been proposed. In one of them, pairing, two eddies approach each other, begin rotating around a common centre and eventually become entangled to form a single eddy (Winant & Browand 1974); during the process new irrotational fluid may or may not be entrained to form the new structure. In the other mechanism, known as tearing, an eddy becomes unstable, disintegrates, and its vorticity is eventually absorbed by its neighbours (Moore & Saffman 1975).

The $(x,t)$-diagram of eddy histories obtained in §4 can be used to distinguish between these two processes. In a pairing two (or more) histories will be found to end while giving rise to a common single descendant, while in a tearing a single history will terminate and, depending upon the speed with which the fluid in the torn eddy is absorbed by its neighbours, it will appear to produce two different descendents (fast interaction), or none at all.

In this way, it is possible to give statistics regarding the relative frequency of the different mechanisms. The simplest way is counting; using only histories beginning or ending in the central part of the image to avoid problems with end effects, we found 96 histories beginning as a consequence of pairings (or triplings), while 20 histories started without an obvious ascendant. These latter histories were interpreted as errors in the tracking algorithm, and a visual inspection in the graphic terminal confirmed that this was generally the case. In this same region 145 histories ended in pairings; assuming an error rate similar to the one above we should expect 30 histories to end abnormally in the region. In fact 36 ended without descendency and 8 with more than one child. The excess of 14 histories over the predicted number is a measure of the relative frequency of tearings versus pairings in this region of the mixing layer (approximately 10 %).

Since the total number of abnormal endings was rather small, a sizable fraction of them could be inspected visually. The results confirm the numbers given above; about two thirds of the cases were tracking errors. In most of the rest the interactions took the form of a slow tearing, or 'bleeding', in which an eddy stopped growing and was slowly absorbed by its neighbours. During this type of interaction the eddies involved usually moved several wavelengths downstream (see figure 10). In only one case did we observe a fast tearing in which an eddy was broken rapidly by its neighbours (figure 11); this was the only fast tearing found, not only in the middle part of the layer but in the whole sequence.

In summary, most of the interactions limiting the life-time of the eddies are

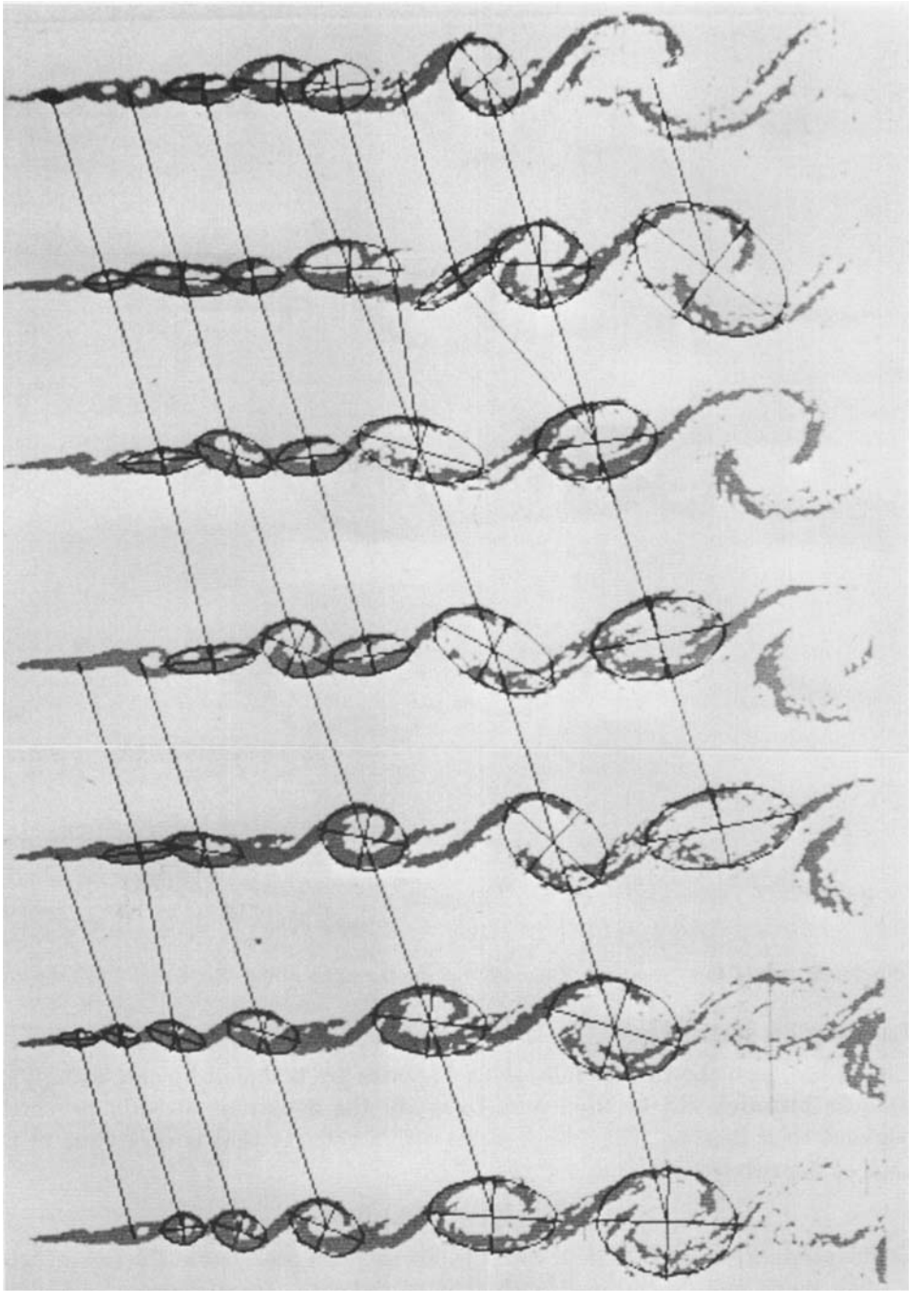

FIGURE 10. A part of the $(x, t)$-diagram showing the disappearance and subsequent 'bleeding' of an eddy. Two independent cases are shown in this picture.

amalgamations; of these most are pairings (196), although triplings are observed on 14 occasions (see figure 7). In 10 % of the cases eddies disintegrate slowly while they are bled by their neighbours. Tearing, on the other hand, seems to occur rather seldom, at least in this experiment.

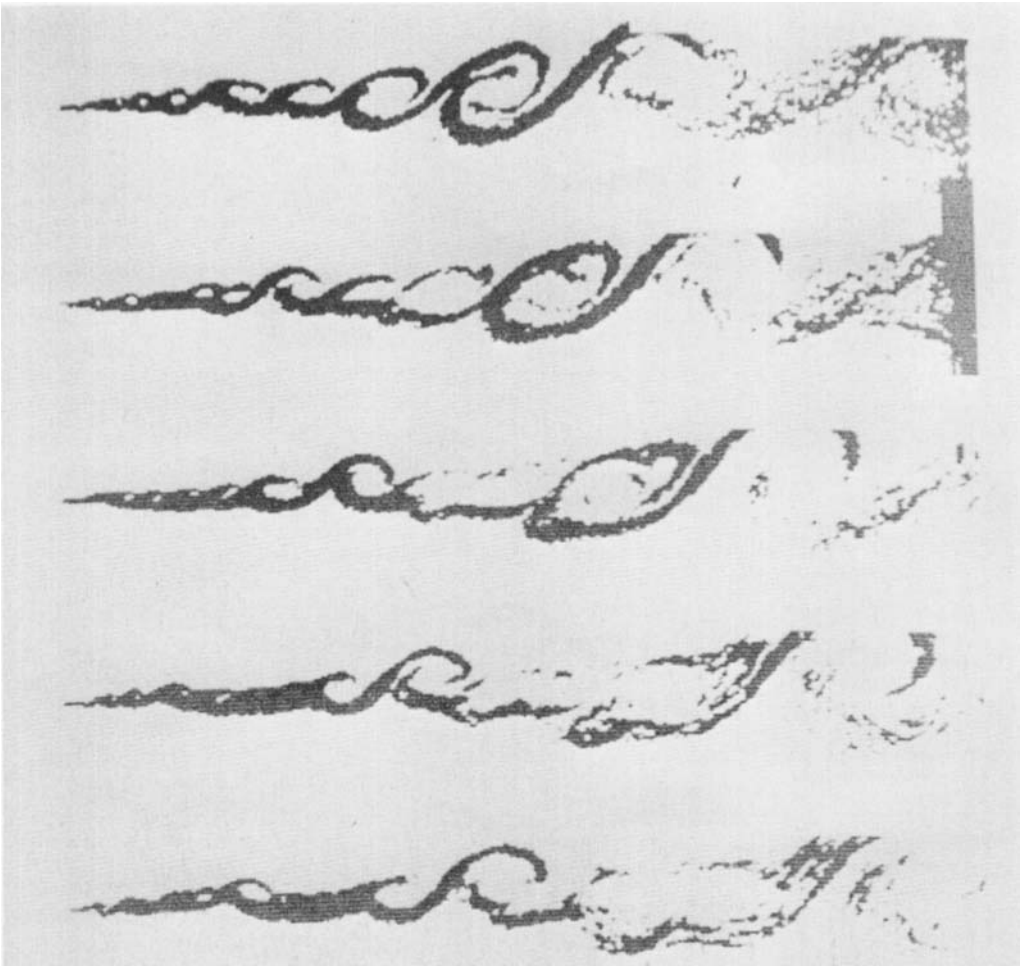

FIGURE 11. A case of fast 'tearing'. The eddy on the far right of the last frame has been torn by the one on its left.

## 7. Lagrangian statistics

Since it has been shown that most eddy histories are bounded by amalgamations, only those histories will be used here to study the evolution of eddy properties throughout their lifetime. The eddies move with a velocity that is very close to the average of the two free streams,

$$U_c/(U_1+U_2) = 0{\cdot}49 \pm 0{\cdot}09. \tag{6}$$

Their lifespans scale approximately with the downstream positions at the time of birth and, when made non-dimensional with that co-ordinate, are distributed according to an exponential distribution (see figure 12) with an average value

$$U_c T/(x_i - x_v) = 0{\cdot}97 \pm 0{\cdot}56. \tag{7}$$

The exponential distribution had been reported before by Roshko (1976), but the average value given here is substantially larger than his measurement (0·43), and agrees better with the ones predicted in Jimenez (1980) on similarity grounds; some consequences of this value will be discussed below.

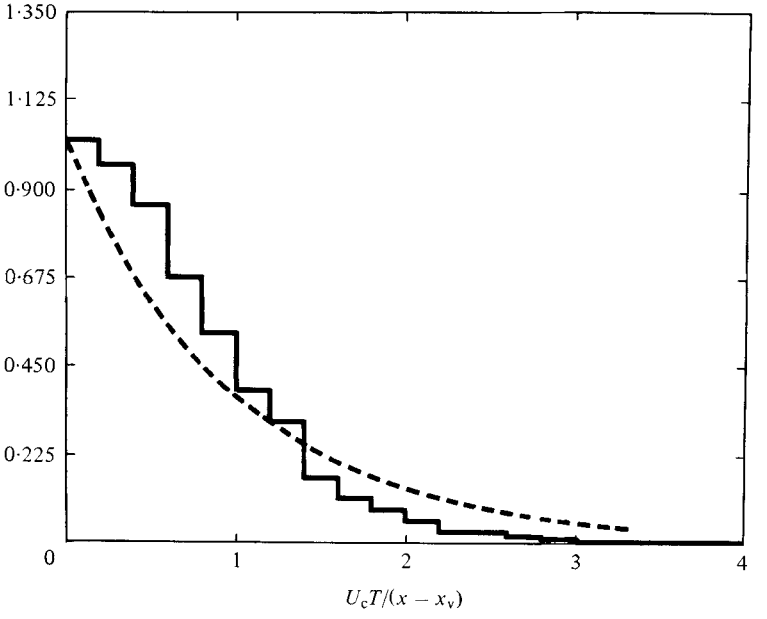


FIGURE 12. Frequency distribution of eddies surviving longer than a given lifespan; sample size = 114.

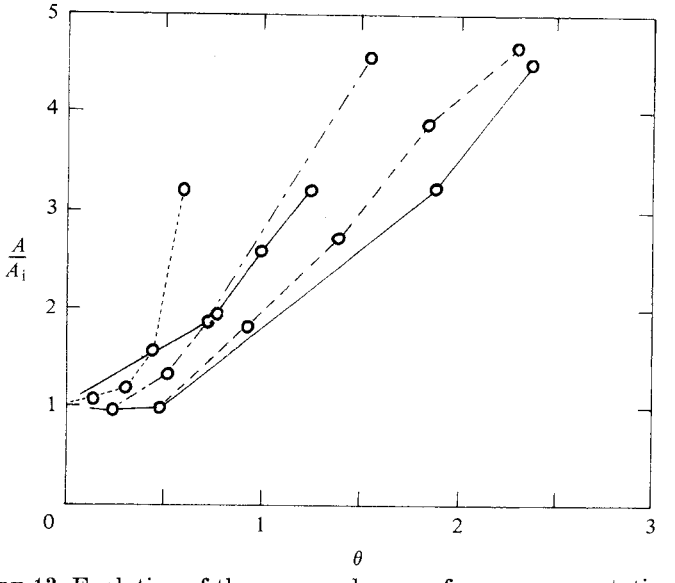


FIGURE 13. Evolution of the measured areas of some representative structures.

The amount of irrotational fluid entrained by the eddies during their evolution can be quantified by measuring the eddy areas. It is observed that, after an initial redistribution period in which the eddy seems to relax from the effects of the pairing interaction and in which there is very little growth, the area increases almost linearly (see figure 13). In fact the growth can be approximated by

$$(A - A_i)/A_i = k_1\theta + k_2[\exp(-\theta) - 1], \tag{8}$$

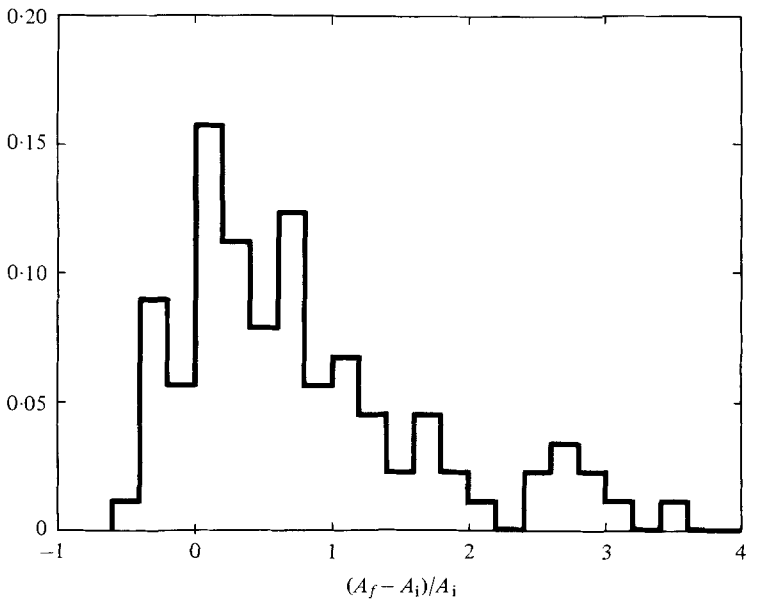


FIGURE 14. Normalized area increase during eddy lifetime, excluding amalgamations; sample size = 177.

where $\theta$ is a non-dimensional time:

$$\theta = U_c(t-t_i)/(x_i-x_v).$$

The slope of the tangent to (8) at the end of the lifetime measures in some way the asymptotic rate of area increase at large times while the time $\theta_T$ at which that tangent crosses the initial area can be taken as representative of the transition between the initial period and the asymptotic growth state. The asymptotic growth rate is distributed normally around the value

$$\frac{1}{A_i}\frac{dA}{d\theta} = 1{\cdot}36 \pm 1{\cdot}54, \tag{9}$$

while the redistribution time follows an exponential distribution with average

$$\theta_T = 0{\cdot}21 \pm 0{\cdot}30. \tag{10}$$

Comparing this latter value with (7) it is seen that the redistribution time, which can actually be considered as part of the pairing process, takes about one-fifth of the total lifespan, while the rest of the time the eddy entrains fluid at an essentially constant rate.

The increase in area over whole lifetimes resulting from this entrainment is represented in figure 14. Some extra fluid is also entrained during the pairing process, and the difference between the area of the eddy resulting from an amalgamation and the sum of the areas of all its parents is given in figure 15. The average value for the first one is

$$(A_f - A_i)/A_i = 0{\cdot}77 \pm 0{\cdot}91, \tag{11}$$

while for the latter it is

$$(A_{aft} - A_{bef})/A_{bef} = 0{\cdot}16 \pm 0{\cdot}46. \tag{12}$$

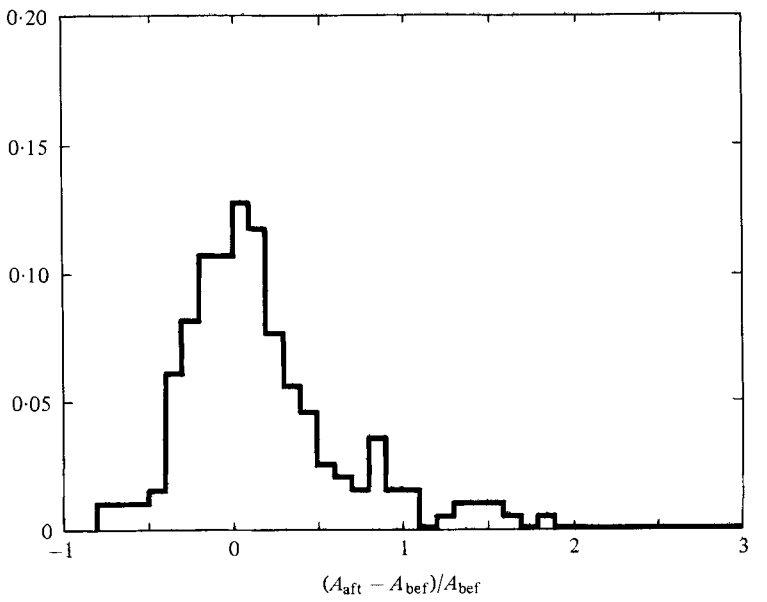


FIGURE 15. Normalized area increase during eddy amalgamation; sample size = 196.

It is clear that in this case most of the entrainment happens by 'passive' eddy growth and that the effect of pairing is relatively minor. This disagrees with some of the early models of mixing-layer growth in which pairing was proposed as the dominant source of entrainment (Winant & Browand 1974), and gives support to models in which fluid is entrained continuously either by irrotational roll-up (Jimenez 1980) or by turbulent diffusion (Moore & Saffman 1975).

These values can be used to check the consistency of the results concerning the frequency of amalgamations (Jimenez, Martinez-Val & Hernan 1981). If the histories interact mainly by pairing, and since there is no intrinsic scale in the problem except for the vorticity contained in each eddy, all linear dimensions should double when measured at equivalent moments of the lifetimes of consecutive generations; in particular, areas should increase by a factor of four. This factor can be measured either from the data in (11) and (12) or directly from the $(x,t)$-diagram. Comparing areas measured just before a pairing with those of the resulting eddy just before it is about to end in the next amalgamation, the result is

$$A_{f+1}/A_f = 4{\cdot}03 \pm 1{\cdot}91, \tag{13}$$

which is in good agreement with the pairing hypothesis. Any amount of vorticity redistribution due to tearing or bleeding would increase this value since the vorticity contained in the teared eddies is used to increase the size of those eddies which are not torn and all scales increase accordingly. Equation (13) is therefore consistent with the result that tearing is a relatively infrequent process.

The average lifespan of eddies can be used in the same way. It can be shown that if the average vorticity per eddy doubles in each generation the non-dimensional lifespan should be equal to unity (Jimenez 1980). Just as before, tearing will increase the vorticity per core and the lifespan; and therefore the value obtained in (7) confirms the conclusions drawn both from the area data and from the amalgamation count.

## 8. Discussion of results

The results presented in the preceding sections pose some constraints on the possible models for the mixing layer. At this point it should be emphasized again that all these results refer only to the evolution of the concentration field and do not necessarily apply to the behaviour of the vorticity in the layer. Thus, even if presumably the general locations of the visual eddies correspond to the vorticity concentrations, it is clear that the detailed shape, size and internal disposition of the two kinds of structures need not be the same. Also, the resolution of the data used here is not enough to investigate the internal structure of the eddies, and it is impossible to decide directly whether irrotational fluid is being entrained by roll-up or by turbulent diffusion, or, equivalently, whether entrainment is led mostly by the large- or the small-scale motions in the flow.

On the other hand we have proved that most of the entrainment occurs during the normal life of the eddies, and not during pairings, and we can compute a magnitude for the sum of entrainment velocities on both sides of the layer. If we assume that the fluid inside the eddies is 'entangled' (although not necessarily mixed at the molecular level), the rate of increase of its area should give this velocity. The areas behave in the average as

$$A = (0{\cdot}441 \pm 0{\cdot}197)\lambda^2, \tag{14}$$

and, using (5), the entrainment velocity can be written as

$$v_e = \frac{d}{dt}\left(\frac{A}{\lambda}\right) = U_c \frac{d}{dx}\left(\frac{A}{\lambda}\right) = 0{\cdot}128(U_1 - U_2). \tag{15}$$

Konrad (1976), using an aspirating probe, has given concentration profiles for a mixing layer that is virtually identical to the one studied here. He measures a total entrainment velocity

$$v_e = \frac{d}{dx}\int_{-\infty}^{\infty} \gamma(y)\, U(y)\, dy = 0{\cdot}158(U_1 - U_2), \tag{16}$$

where $\gamma$ is the intermittency factor, defined as the probability of finding 'entangled' fluid at a given point. This velocity should correspond to the one above, and its measured value does indeed coincide approximately with (15).

In fact, assuming that all the entangled fluid is inside the visual eddies, it is possible to compute the intermittency factor from the statistics of eddy shape. Consider figure 16, which represents the region in between two eddies; the two wedges near the centre contain all the pure fluid, and the probability of finding entangled fluid at a given position across the layer is

$$\gamma(y) = 2X(y)/\lambda. \tag{17}$$

The statistics for the eddy semi-axis are

$$a/\lambda = 0{\cdot}497 \pm 0{\cdot}145, \quad b/\lambda = 0{\cdot}270 \pm 0{\cdot}070, \tag{18}$$

and the resulting intermittency is represented as a solid line in figure 17. The symbols in that figure are experimental values given by Konrad, and the transverse dimension has been normalized using his measured vorticity thickness; the agreement between the two sets of data is quite good, especially considering the differences between the

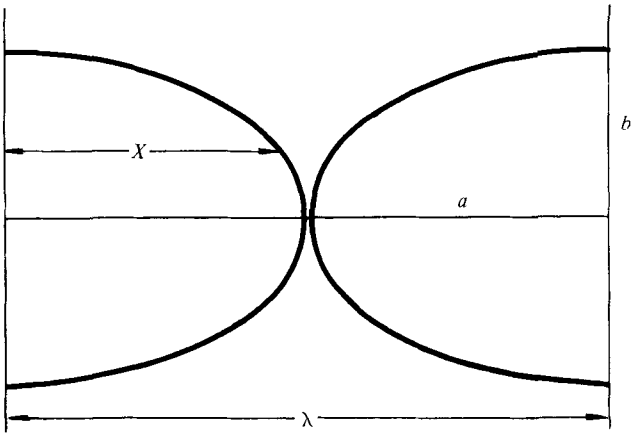


FIGURE 16. A sketch of the region between two large eddies. The fluid inside the ellipses is assumed to be 'entangled', while that outside is pure. Dimensions are average values obtained from the data.

two techniques. Actually, the remaining discrepancy can be reduced by introducing the lateral scatter of the eddies around the centre line. If the probability distribution of this scatter is $p(y)$, a better approximation for the intermittency is

$$\gamma(y) = \frac{2}{\lambda}\int_{-\infty}^{\infty} p(y')\, X(y-y')\, dy'. \tag{19}$$

Assuming that the distribution is Gaussian, and taking the variance from (2), we get the dashed line in figure 17, which agrees very well with Konrad's measurements.

Another striking fact is the amount of deterministic behaviour present in the layer. The large eddies seem to behave most of the time like solid structures deforming slowly and moving at a constant velocity. The peaks in the distribution of wavelengths (figure 9) imply that, at least at the beginning, eddies are very similar to one another, and it is only later that disorder is introduced in the layer. The main form of interaction is pairing, and this allows us to think of eddies as going through a series of generations, in each of which their dimensions and lifespan double. This quasi-deterministic model has been used already in the analysis of (7) and (13); we will show here that it can be used to derive other properties. Assume that the initial instability creates eddies with wavelength $\lambda_0$ and that the first pairing occurs, in the average, at position $2x_0$; since in one lifespan an eddy moves on amount roughly equivalent to its position at birth (equation (7)) the $n$th pairing will be expected to occur at $x_n = 2^n x_0$. The number of pairings per unit time associated with each generation decreases because the number of eddies is cut by half at each pairing; at the $n$th generation we will expect $U_c/2^n\lambda_0$ pairings, and we can assume that they will happen in the space between the midpoints of the lifetimes immediately before and behind it. The length of this segment is $3x_0 2^{n-2}$, and therefore the spatial density of pairing will be given by

$$d_n = 4U_c 2^{-2n}/3x_0\lambda_0 = 4U_c x_0/3\lambda_0 x_n^2. \tag{20}$$

Associating $\lambda_0$ with the midpoint of the first lifetime $\frac{3}{2}x_0$, and using (5), we get for the pairing density

$$d = 1{\cdot}538U_c/\alpha x^2. \tag{21}$$

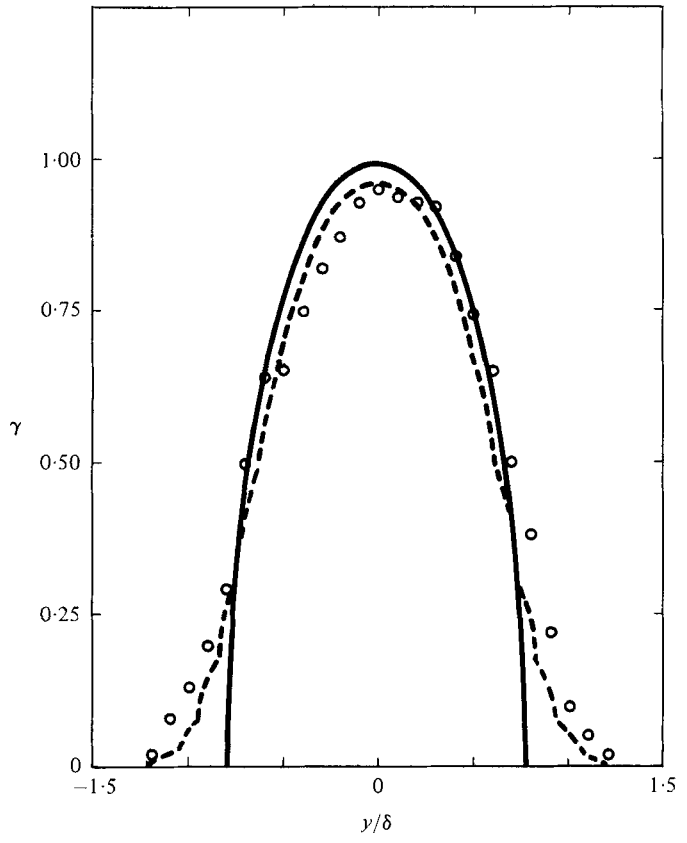


FIGURE 17. Intermittency factor for the concentration distribution. Solid line is derived from model in text without scatter; dashed line is the result of model taking scatter into account. Symbols are measurements from Konrad (1976).

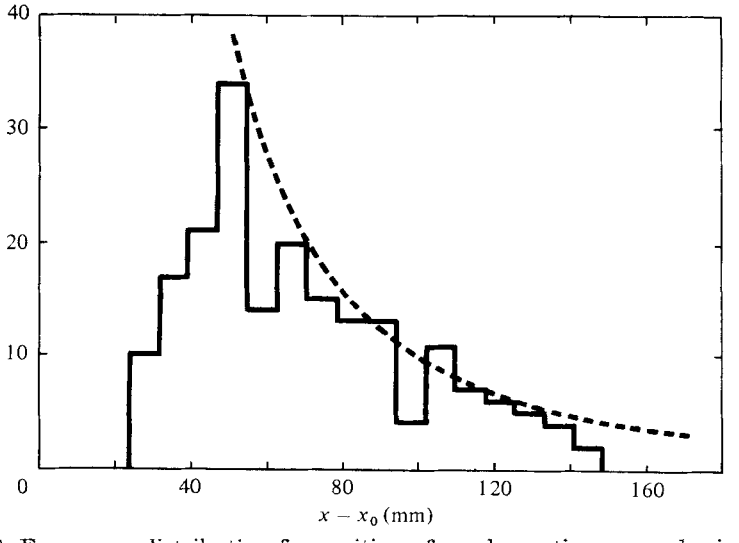


FIGURE 18. Frequency distribution for position of amalgamations; sample size = 196. Line is derived from model in text.

This function, together with the observed values of pairing density, are shown in figure 18. For laminar initial boundary layers the value of $x_0$ is approximately $50\delta_2/\alpha$, where $\delta_2$ is the momentum thickness of the boundary layer at the high-speed side of the splitter plate (Jimenez *et al.* 1979*b*), so that the $n$th pairing will happen near

$$x_n = 50\delta_2 2^n/\alpha. \tag{22}$$

The same functional relation was given in Dimotakis & Brown (1976), where it was pointed out that it implies that, in most practical layers, there are just a few eddy generations, and that it will take a long time for the flow to attain equilibrium. This is especially true if we believe the randomization mechanism discussed in §5, by which the disorder arises from non-uniformities in the amalgamation process. As an example it is interesting to realize that the whole section of mixing layer studied in this paper contains somewhat less than two complete life-cycles (figure 18).

Before concluding this analysis it is important to notice two limitations of the data presented here. The first arises from the fact that only a single ciné film has been studied; as a consequence the non-dimensional form given for some quantities is arbitrary. In particular, since the only other reliable measurements of eddy wavelengths and lifespans refer either to layers with very similar velocity ratios (Winant & Browand 1974; Roshko 1976) or to flows that do not necessarily behave in the same way (round jets), there is little experimental support for the dependence on the velocity ratio given in (5) and (7). The expressions used here are chosen to be consistent with a particular theoretical model (Jimenez 1980). The same can be said about the Reynolds-number dependence; Saffman (1980) has suggested that eddy interaction should happen first by amalgamation, and that tearing will only be important after a few generations have occurred. The fact that we have found hardly any tearing in this experiment is, of course, not inconsistent with this possibility. Clearly it is desirable to study more cases to clarify these questions.

Finally, it should be noted that the shadowgraph technique used in this film integrates the information along the span of the layer. This is specially important since recent evidence indicates that the concentration field may have strong variations along that direction (Roshko 1980), pointing to the desirability of comparing the results of this analysis with some other film obtained by more discriminating diagnostic techniques.

## 9. Conclusions

In §8 we have summarized the consequences of the data obtained in this paper from the point of view of the mixing-layer models. Here we make some considerations on the method of analysis itself. We have shown that the quantitative analysis of flow pictures can be used to obtain much of the same information usually associated with classical point probes. Moreover, when the same quantity is measured using both methods the results usually agree. On the other hand, much of the data presented in this paper could not have been obtained from point measurements; this is especially true of the shape and size information and of the Lagrangian statistics in which a single extended object is followed in time. In some of these cases the contribution of automatic signal processing has been crucial.

One consideration is cost. Many of the operations of enhancement and display can

be done by purely photographic means and, given a proper display method, much of the subsequent analysis can be done by a human operator; the effort needed to do this for a large number of frames is, however, not trivial.

Our analysis was done using a large computer and relatively large virtual machines (500 kbytes), but most of the programs could be run on a smaller system. By far the longest processes were the digitization of the film and the production of software. For the digitization, even if most of the process is automatic, the initial positioning of the frame in the scanner must be done by the operator; the scanning of each frame takes about five minutes. On the question of software this project is somewhat atypical. Since the goal was not only to solve a problem in fluid mechanics but to develop techniques in image processing, many of the programs that would normally be taken from a library were written from scratch; also an effort was made to test the limits of the algorithms beyond, in many cases, what was actually needed for the problem at hand. The development of the software took about a year and is part of the doctoral thesis work of one of the authors (M. A. H.). Much of this software, in particular most of the preprocessing and display, is of a general nature and will not have to be written again for a new application. The rest – segmentation, time-correlation and statistical analysis of the data – is specific and represents the real investment dedicated to the project.

The preprocessing of the images took 12 s/CPU per frame on an IBM 370/158, rated at approximately one Mip (Mega instructions per second), while the subsequent processing of the whole sequence needed a total of some 25 minutes. These are moderate times for normal data-processing applications.

Some comment should be made on the relation between interactive and fully automatic programs. Most of the algorithms in this work were written in both versions. The automatic version was always used for final production, while the interactive one was used to monitor the correct functioning of the programs, to fine-tune the parameters, and in one case to train the computer and to get a 'feeling' of the problem at hand. All of these activities are important and constitute a necessary link between the computer and the investigator; the last one is perhaps especially so. In this case the computer is being used essentially as a tool to point to the operator the interesting cases so that he can decide which action to take. One clear example is the discovery of the 'bleeding' interaction described in §6. In this case the main use of the computer was to reduce the original set of 373 frames to a smaller one of 36 that were already labelled as interesting and ready for visual analysis. It is perhaps true that most of the applications of image processing are of this type, and this is almost certainly so in the analysis of a small number of pictures; there are cases, however, in which fully automatic processing is needed.

The analysis of ciné films is one such case. The factor of cost has been mentioned before, but perhaps a more important reason is consistency and objectivity. It is difficult for a human operator to keep a consistent criterion in processing a large set of pictures over several days; it is still harder not to be unconsciously biased during that time to see in the data what one wants to find. Automatic analysis is, of course, not entirely free of the observer-bias problem, since the output will depend on how the program is written, but the effort to write a precise algorithm in an unfamiliar language does help in keeping objectivity intact. Consistency, on the other hand, is assured almost completely.

In general, we feel that interactive image processing can become a very important tool in the analysis of visual information on flows. We also think that, as the cost of computers and scanners comes down, fully automatic analysis will become an increasingly large part of this processing, especially for those activities involving repetitive work and the compilation of statistics. Even now, as long as an appropriate scanner and display are available, the cost can be kept within reasonable limits which compete favourably with other types of processing.

One of the authors (M. A. H.) wishes to acknowledge the partial support by an IBM Scientific Center fellowship during the course of this work.

## REFERENCES

BROWN, G. L. & ROSHKO, A. 1974 On density effects and large structure on turbulent mixing layers. *J. Fluid Mech.* **64**, 775–816.

CHOW, C. K. & KANEKO, T. 1972 Boundary detection of radiographic images by a threshold method. In *Frontiers in Pattern Recognition* (ed. S. Watanabe), pp. 61–82. Academic.

DIMOTAKIS, P. E. & BROWN, G. L. 1976 The mixing layer at high Reynolds number: large-structure dynamics and entrainment. *J. Fluid Mech.* **78**, 535–560.

FU, K. S. 1974 *Syntactic Methods in Pattern Recognition.* Academic.

JIMENEZ, J. 1980 On the visual growth of a turbulent mixing layer. *J. Fluid Mech.* **96**, 447–460.

JIMENEZ, J., MARTINEZ-VAL, R. & HERNAN, M. A. 1981 Shear layer models and computer analysis of data. In *The Role of Coherent Structures in Modelling Turbulence and Mixing* (ed. J. Jimenez). Lecture Notes in Physics, vol. 136, pp. 41–61. Springer.

JIMENEZ, J., MARTINEZ-VAL, R. & REBOLLO, M. 1979*a* The spectrum of large scale structure in a mixing layer. In *Proc. 2nd Symp. on Turbulent Shear Flows, London*, pp. 8.7–8.11.

JIMENEZ, J., MARTINEZ-VAL, R. & REBOLLO, M. 1979*b* On the origin and evolution of three dimensional effects in the mixing layer. *Universidad Politecnica de Madrid Final Report*, DA-ERO 79-G-079.

KONRAD, J. H. 1976 An experimental investigation of mixing in two-dimensional turbulent shear flows with application to diffusion-limited chemical reactions. Ph.D. thesis, California Institute of Technology. *Tech. Rep.* CIT-8-PU.

KOOCHESFAHANI, M. M., CATHERASOO, C. J., DIMOTAKIS, P. E., GHARIB, M. & LANG, D. B. 1979 Two-point LDV measurements in a plane mixing layer. *A.I.A.A. J.* **17**, 1347–1351.

MOORE, D. W. & SAFFMAN, P. G. 1975 The density of organized vortices in a turbulent mixing layer. *J. Fluid Mech.* **69**, 465–473.

PAVLIDIS, T. 1977 *Structural Pattern Recognition.* Springer.

PRATT, W. K. 1978 *Digital Image Processing.* Wiley.

ROSHKO, A. 1976 Structure of turbulent shear flows: a new look. *A.I.A.A. Paper* no. 76-78.

ROSHKO, A. 1980 The plane mixing layer, flow visualization results and three dimensional effects. In *The Role of Coherent Structures in Modelling Turbulence and Mixing* (ed. J. Jimenez). Lecture Notes in Physics, vol. 136, pp. 208–217. Springer.

SAFFMAN, P. G. 1980 Vortex interactions and coherent structures in turbulence. In *Proc. Symp. on Transition and Turbulence, Madison.* Academic.

TOWNSEND, A. A. 1956 *The Structure of Turbulent Shear Flow*, Cambridge University Press.

WINANT, C. D. & BROWAND, F. K. 1974 Vortex pairing: the mechanism of turbulent mixing-layer growth at moderate Reynolds number. *J. Fluid Mech.* **63**, 237–255.

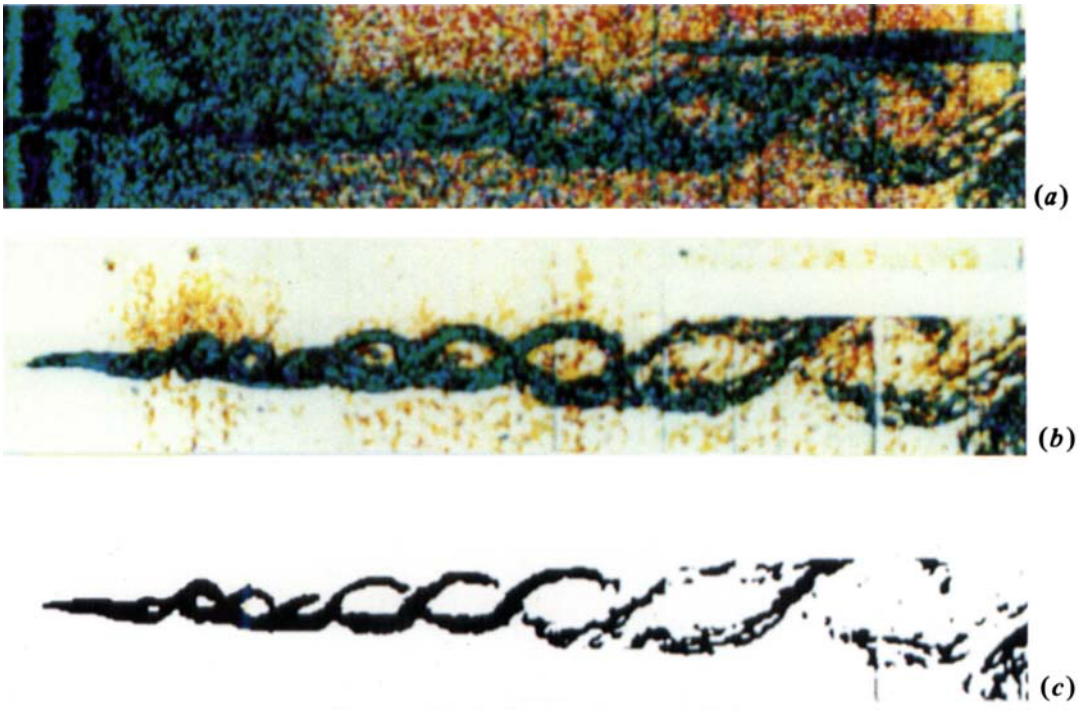


FIGURE 2(*a–c*). See caption on p. 327.

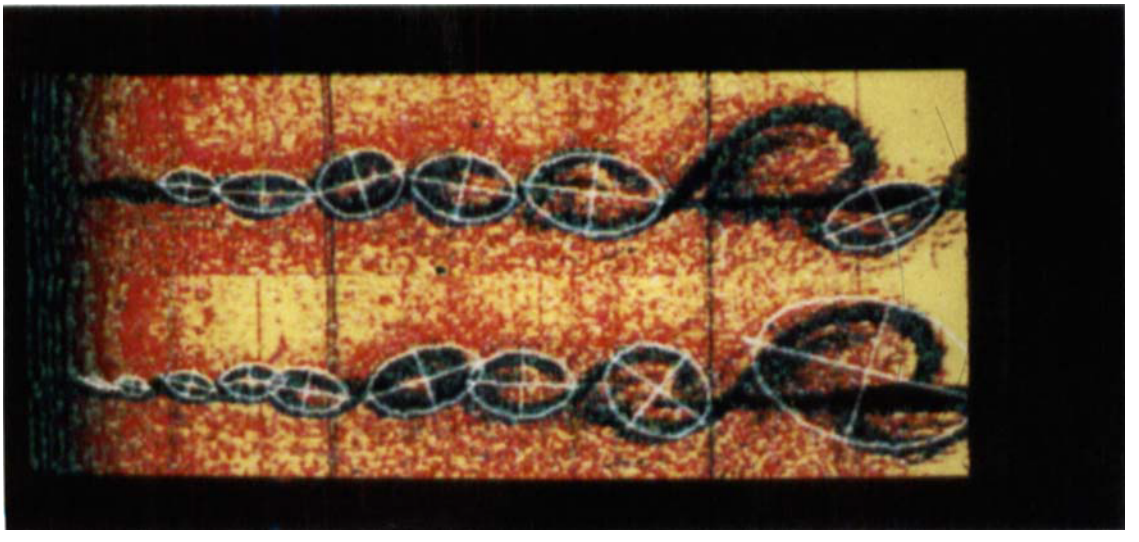

FIGURE 4. The result of image segmentation and ellipse fitting for two consecutive frames.